Article

SOURCE DATA | TRANSPARENT PROCESS

THE EMBO JOURNAL

# Ubiquitin-specific protease USP34 controls osteogenic differentiation and bone formation by regulating BMP2 signaling

Yu-chen Guo†, Meng-yuan Wang†, Shi-wen Zhang†, Yun-shu Wu, Chen-chen Zhou, Ri-xin Zheng, Bin Shao, Yuan Wang, Liang Xie, Wei-qing Liu, Ning-yuan Sun, Jun-jun Jing, Ling Ye, Qian-ming Chen & Quan Yuan*

## Abstract

**The osteogenic differentiation of mesenchymal stem cells (MSCs) is governed by multiple mechanisms. Growing evidence indicates that ubiquitin-dependent protein degradation is critical for the differentiation of MSCs and bone formation; however, the function of ubiquitin-specific proteases, the largest subfamily of deubiquitylases, remains unclear. Here, we identify USP34 as a previously unknown regulator of osteogenesis. The expression of USP34 in human MSCs increases after osteogenic induction while depletion of USP34 inhibits osteogenic differentiation. Conditional knockout of Usp34 from MSCs or pre-osteoblasts leads to low bone mass in mice. Deletion of Usp34 also blunts BMP2-induced responses and impairs bone regeneration. Mechanically, we demonstrate that USP34 stabilizes both Smad1 and RUNX2 and that depletion of Smurf1 restores the osteogenic potential of Usp34-deficient MSCs *in vitro*. Taken together, our data indicate that USP34 is required for osteogenic differentiation and bone formation.**

**Keywords** bone formation; mesenchymal stem cells; osteogenic differentiation; ubiquitin-specific protease 34

**Subject Categories** Development & Differentiation; Post-translational Modifications, Proteolysis & Proteomics; Signal Transduction

**DOI** 10.15252/embj.201899398 | Received 7 March 2018 | Revised 30 July 2018 | Accepted 13 August 2018 | Published online 4 September 2018

**The EMBO Journal (2018) 37: e99398**

## Introduction

Mesenchymal stem cells (MSCs) are heterogeneous progenitors which self-renew and differentiate into multiple lineages of mesenchymal tissues, including bone, fat, cartilage, tendon, and muscle (Caplan, 1991; Pittenger *et al*, 1999; Sacchetti *et al*, 2007; Bianco *et al*, 2008; Mendez-Ferrer *et al*, 2010). They have been identified and isolated from various tissues such as bone marrow, adipose tissue, umbilical cord blood, and dental tissues (Pittenger *et al*, 1999; Lee *et al*, 2004; Schaffler & Buchler, 2007; Sharpe, 2016). The intrinsic properties of MSCs make them an attractive candidate for clinical regenerative therapies (Caplan, 2007; Grayson *et al*, 2015; Malhotra *et al*, 2016).

The skeleton undergoes continuous remodeling with resorption by osteoclasts and formation by osteoblasts which are derived from MSCs (Zaidi, 2007; Crane & Cao, 2014). The process of MSC osteogenic differentiation begins with osteoprogenitor commitment followed by differentiation to pre-osteoblasts and eventually development to mature osteoblasts (James, 2013). Disruption of this process leads to improper bone formation and imbalanced skeletal homeostasis. Mechanically, the osteogenic differentiation of MSCs is governed by master transcriptional factors, such as runt-related gene 2 (RUNX2) and osterix (SP7), as well as by extrinsic regulators, such as cytokines, growth factors, and systemic hormones (Frith & Genever, 2008; Raggatt & Partridge, 2010; Yuan *et al*, 2014). In addition, there is growing evidence indicates that ubiquitin-dependent proteolysis is crucial for the fine tuning of MSC differentiation.

The ubiquitination system is an enzymatic cascade that adds ubiquitin chains to target proteins and thereby directs their degradation (Ciechanover, 2005). Ubiquitination is carried out by ubiquitin-activating enzymes (E1), ubiquitin-conjugating enzymes (E2), and ubiquitin ligases (E3), which is the most abundant group of enzymes involved in ubiquitination (Komander, 2009). The ubiquitination process is reversible through the action of deubiquitinases that remove ubiquitin marks (Komander *et al*, 2009). Significant progress has been made in understanding the molecular regulation of MSC differentiation by ubiquitin ligases (Severe *et al*, 2013; Vriend & Reiter, 2016). For example, the E3 enzyme Smurf1 mediates the degradation of RUNX2, MEKK2, and JunB, resulting in inhibition of osteoblast differentiation and bone formation (Zhao *et al*, 2003, 2010; Yamashita *et al*, 2005). However, very little is known about the role of deubiquitinases in regulating MSC commitment.

State Key Laboratory of Oral Diseases, National Clinical Research Center for Oral Diseases, West China Hospital of Stomatology, Sichuan University, Chengdu, China
*Corresponding author. Tel: +86 28 8550 1441; E-mail: yuanquan@scu.edu.cn
†These authors contributed equally to this work

The ubiquitin-specific protease (USP) family, which consists of nearly 60 known members, is the largest of five families of deubiquitylases. These families are organized by the architecture of their catalytic domains (Liu *et al*, 2016a). It has been suggested that a few USPs, such as USP1 and USP6, are involved in preserving a mesenchymal stem cell program or antagonizing osteoblast differentiation (Williams *et al*, 2011; Zhou *et al*, 2016). Here, we screen the members of USP family and identify USP34 as a previously unknown regulator of osteogenesis. Conditional knockout of *Usp34* leads to low bone mass in mice, blunted responses to BMP2, and impaired bone regeneration. Mechanically, we demonstrate that USP34 stabilizes both Smad1 and RUNX2.

## Results

### USP34 is required for osteogenic differentiation of MSCs

To investigate the potential role of USPs in osteogenesis, we first profiled the expression of 54 known USPs in MSCs after osteogenic induction. Human bone marrow MSCs were depleted with serum overnight and then treated with a combination of 100 ng/ml BMP2 and 100 ng/ml Wnt3a, which are critical regulators for osteogenic differentiation and synergistically activate the transcription of osteogenic genes to stimulate new bone formation (Rodriguez-Carballo *et al*, 2011). Quantitative reverse transcriptase-polymerase chain reaction (RT–PCR) revealed that *USP34*, together with *USP13*, *USP18*, *USP21,* and *USP53*, were the top five genes induced by the treatment (Appendix Fig S1A–C).

Next, we sought to investigate whether these 5 USPs are required for the osteogenic differentiation of MSCs by loss-of-function method using small interfering RNAs (siRNAs; Appendix Fig S2A and B). After culturing with osteogenic induction medium for 5 days, the intensities of alkaline phosphatase (ALP) and Van Gieson's staining were markedly reduced upon *USP34* knockdown (Fig 1A). Moreover, *USP34* depletion reduced the formation of mineralized nodules after osteogenic induction for 2 weeks (Fig 1A). These observations were confirmed by quantitative analyses of ALP activity (Fig 1B) and calcium mineralization (Fig 1C). *USP34* knockdown also resulted in decreased expression of the master osteogenic transcription factors and markers, such as *DLX5*, *RUNX2*, *ATF4*, *SP7*, *COL1A1*, *SPP1,* and *BGLAP* (Fig 1D and E). However, depletion of *USP13*, *USP18*, *USP21,* or *USP53* did not affect the osteogenic potential of human MSCs (Appendix Fig S2C–F).

In addition, we generated stable knockdown human MSCs using lentiviruses expressing shRNA and implanted them with β-TCP carriers into immunocompromised mice subcutaneously. The knockdown efficiency was confirmed by quantitative RT–PCR and Western blot (Appendix Fig S2G and H). H&E staining showed that USP34-depleted cells formed much less bone tissue (Fig 1F) when compared with control cells that had scrambled shRNA. Quantitative measurement of newly formed bone area revealed a 35% reduction (Fig 1G).

### Conditional deletion of *Usp34* in MSCs leads to low bone mass

To further investigate the role of USP34 *in vivo*, we performed immunohistochemical staining of USP34 on mouse femoral sections and observed that USP34 is widely expressed in bone marrow cells, osteoblasts, osteocytes, and hypertrophic chondrocytes of the growth plate (Appendix Fig S3A). We also generated *Prx1-Cre;tdTomato* mice and sorted the Tomato$^+$ cells (Appendix Fig S3B). Interestingly, the expression of Usp34 was decreased in Tomato$^+$ cells isolated from aged mice compared to those from young adults (Appendix Fig S3C and D), suggesting a potential role of USP34 in age-related osteoporosis.

Next, we generated *Usp34* floxed (*Usp34*$^{f/+}$) mice using CRISPR/Cas9 (Appendix Fig S4A). LoxP sites were integrated into the *Usp34* allele flanking the second exon, which contains the start codons of all known *Usp34* isoforms. Cre recombinase-mediated removal of exon 2 is thus expected to cause a translation termination of *Usp34.* We then bred *Usp34*$^{f/+}$ mice with *Prx1-Cre* transgenic mice to conditionally delete *Usp34* from MSCs (Appendix Fig S4A and B). Prx1 is a transcription factor expressed during early limb bud mesoderm development; therefore, Prx1-Cre targets all cells derived from limb bud mesoderm (Logan *et al*, 2002). The knockout efficiency was confirmed by quantitative RT–PCR and Western blot (Appendix Fig S4C and D). *Prx1-Cre;Usp34*$^{f/f}$ mice were viable and born at the expected Mendelian ratio. The body size and weight of *Prx1-Cre;Usp34*$^{f/f}$ mice were comparable to their littermate controls (Appendix Fig S4E and F).

MicroCT analysis of trabecular bone from the distal femur metaphysis revealed that the bone mineral density (BMD) and bone volume (BV/TV) in *Prx1-Cre;Usp34*$^{f/f}$ male mice were significantly lower than those of their *Usp34*$^{f/f}$ littermates (Fig 2A and C). *Prx1-Cre;Usp34*$^{f/f}$ mice also had reduced trabecular number (Tb.N), decreased trabecular thickness (Tb.Th), and increased trabecular separation (Tb.Sp) (Fig 2C). Von Kossa staining of undecalcified sections further confirmed the decrease in trabecular bone in *Prx1-Cre;Usp34*$^{f/f}$ mice (Fig 2B).

Bone homeostasis is dependent on the coupling of bone formation and resorption (Sims & Martin, 2014). To unveil the cellular basis for decreased bone mass in *Prx1-Cre;Usp34*$^{f/f}$ mice, we performed the histomorphometric analysis. Osteoblast numbers (N.Ob/B.Pm) were significantly reduced, while osteoclast numbers (N.Oc/B.Pm) were unchanged (Fig 2C). Meanwhile, the mineral apposition rate (MAR) and bone formation rate (BFR/BS) in *Prx1-Cre;Usp34*$^{f/f}$ mice were both significantly lower than in the controls (Fig 2C), indicating a reduction in bone formation. We also performed ELISA to assess the serum markers for bone turnover. The serum levels of the bone formation marker P1NP were reduced in 6-week-old *Prx1-Cre;Usp34*$^{f/f}$ mice, whereas the levels of c-terminal telopeptides of collagen type I (CTX), a marker for bone resorption, were not affected (Fig 2D). We excluded the potential difference between sexes by thoroughly examining the skeletal phenotype of female animals and observed a similar reduction in bone formation (Appendix Fig S5A–D).

Next, we obtained the femoral bone samples from *Usp34*$^{f/f}$ and *Prx1-Cre;Usp34*$^{f/f}$ mice and performed quantitative RT–PCR analyses. The expression of osteogenic markers, such as *Dlx5*, *Runx2*, *Atf4*, *Sp7*, *Col1a1*, *Spp1,* and *Bglap*, were significantly decreased, while those of *Rankl*, *Opg, Axin1, Axin2, Dkk1,* and *β-catenin* was unchanged (Fig 2E and Appendix Fig S6). We also isolated the bone marrow MSCs from *Usp34*$^{f/f}$ and *Prx1-Cre;Usp34*$^{f/f}$ mice and

 

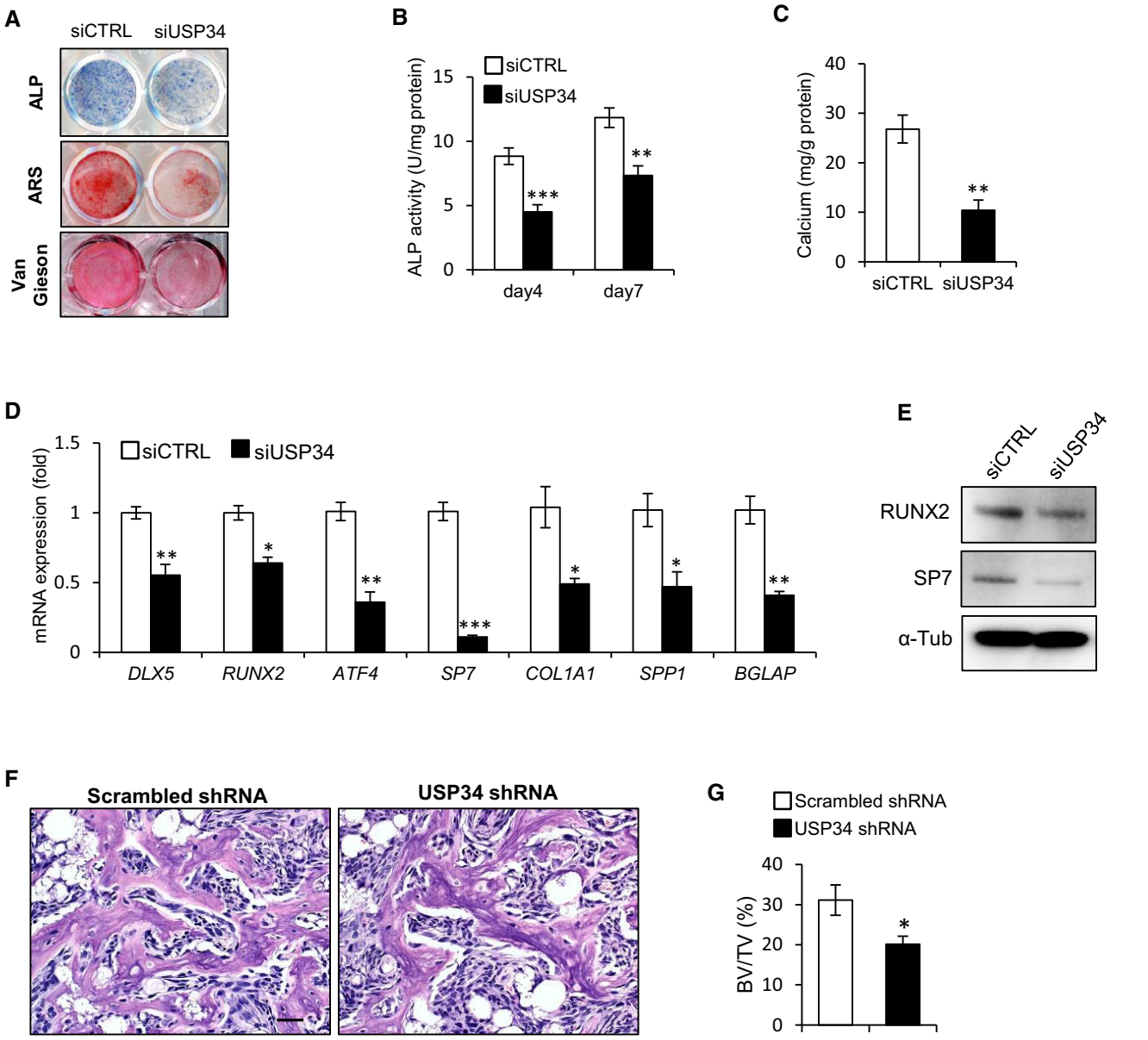


**Figure 1. USP34 is required for osteogenic differentiation of human MSCs.**

A Representative images of alkaline phosphatase (ALP), alizarin Red S (ARS), and Van Gieson's staining of human MSCs.

B, C Quantitative analyses of the ALP activity and calcium mineralization. Results are shown as mean ± SEM; $n = 6$; $^{**}P < 0.01$ and $^{***}P < 0.001$ by $t$-test.

D, E Quantitative RT–PCR and Western blot analyses of the expression of osteogenic markers. Cells were cultured in osteogenic medium for 5 days. Results are shown as mean ± SEM; $n = 3$; $^{*}P < 0.05$, $^{**}P < 0.01$, and $^{***}P < 0.001$ by $t$-test.

F H&E staining of the MSC-mediated ectopic bone formation. Scale bar, 50 μm.

G Quantitative analysis of bone volume versus total tissue volume (BV/TV). Results are shown as mean ± SEM; $n = 6$. $^{*}P < 0.05$ by $t$-test.

Source data are available online for this figure.

compared their osteogenic potential *in vitro*. *Prx1-Cre;Usp34*$^{f/f}$ MSCs exhibited inhibited osteogenic differentiation, as evidenced by decreased ALP activity, calcium mineralization, collagen synthesis, and osteogenic marker gene expression (Fig 2F–I). Similar results were also observed in primary calvarial osteoblasts (Fig 2J–M).

### Conditional deletion of *Usp34* in pre-osteoblasts impairs bone formation

To further investigate whether deletion of Usp34 from committed osteoblast progenitors could recapitulate similar bone loss, we used Sp7-Cre, which recombines efficiently in pre-osteoblasts (Rodda &

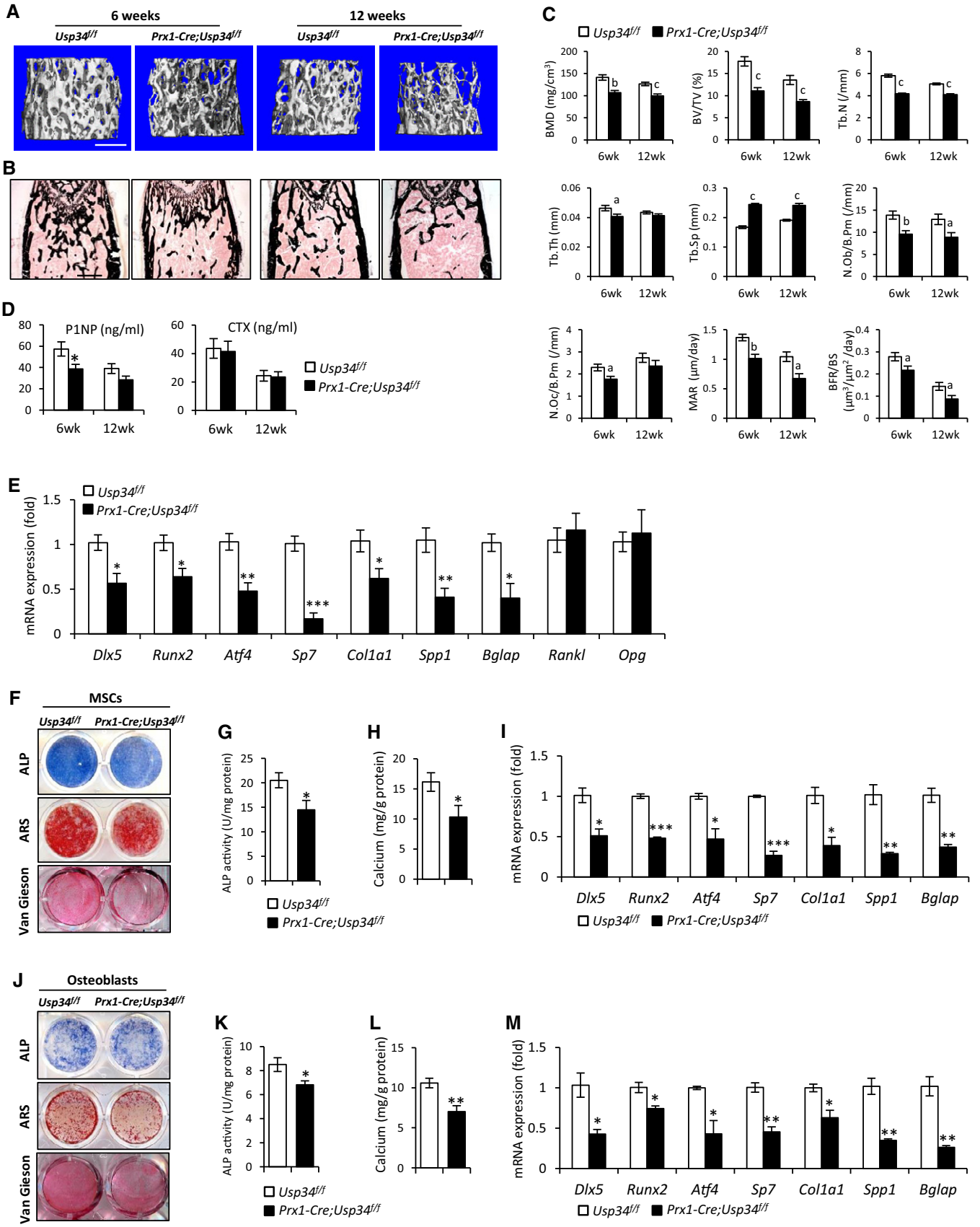


**Figure 2.**

**Figure 2. Conditional deletion of *Usp34* in MSCs leads to low bone mass.**

A Representative microCT images of trabecular bone from the femoral metaphysis of male *Prx1-Cre;Usp34$^{f/f}$* and littermate control mice. Scale bar, 500 μm.

B Von Kossa staining of undecalcified sections of femurs. Scale bar, 500 μm.

C Histomorphometric analysis of trabecular bone from the femoral metaphysis. Results are shown as mean ± SEM; $n = 8$; a: $P < 0.05$, b: $P < 0.01$, and c: $P < 0.001$ by *t*-test.

D Serum levels of P1NP and CTX. Results are shown as mean ± SEM; $n = 8$; $^*P < 0.05$ by *t*-test.

E Quantitative RT–PCR analyses of the gene expression of femoral bone samples. Results are shown as mean ± SEM; $n = 6$; $^*P < 0.05$, $^{**}P < 0.01$, and $^{***}P < 0.001$ by *t*-test.

F Representative images of ALP, ARS, and Van Gieson's staining of MSCs obtained from *Prx1-Cre;Usp34$^{f/f}$* and littermate control mice.

G, H Quantitative analyses of the ALP activity and calcium mineralization of MSCs. Results are shown as mean ± SEM; $n = 6$; $^*P < 0.05$ by *t*-test.

I Quantitative RT–PCR analyses of the transcription of osteogenic markers. MSCs were differentiated in osteogenic medium for 5 days. Results are shown as mean ± SEM; $n = 3$; $^*P < 0.05$, $^{**}P < 0.01$, and $^{***}P < 0.001$ by *t*-test.

J Representative images of ALP, ARS, and Van Gieson's staining of primary calvarial osteoblasts.

K, L Quantitative analyses of the ALP activity and calcium mineralization of primary calvarial osteoblasts. Results are shown as mean ± SEM; $n = 6$; $^*P < 0.05$ and $^{**}P < 0.01$ by *t*-test.

M Quantitative RT–PCR analyses of the transcription of osteogenic markers. Calvarial osteoblasts were differentiated in osteogenic medium for 5 days. Results are shown as mean ± SEM; $n = 3$; $^*P < 0.05$ and $^{**}P < 0.01$ by *t*-test.

McMahon, 2006). *Sp7-Cre;Usp34$^{f/f}$* mice exhibited normal Mendelian inheritance and growth features. MicroCT analysis revealed an impairment in trabecular bone micro-architecture, as measured by reduced skeletal parameters of BMD, BV/TV, and Tb.N and increased Tb.Sp, in the femur metaphysis of both male and female *Sp7-Cre;Usp34$^{f/f}$* mice (Fig 3A–F). In addition, the decline in osteoblast numbers and dynamic bone histomorphometry characteristics consolidated the osteopenic phenotype of mutant mice (Fig 3A–F).

*Sp7-Cre;Usp34$^{f/f}$* MSCs also showed an equivalent resistance to osteogenic differentiation as seen with *Prx1-Cre*-driven *Usp34*-ablated MSCs. Knockout of *Usp34* inhibited ALP activity, collagen synthesis, mineralization, and expression of osteogenic marker genes *in vitro* (Fig 3G–J), establishing the essentiality of Usp34 as a regulator during osteogenic lineage commitment.

### Loss of USP34 attenuates BMP2 signaling

Next, we sought to elucidate the molecular mechanism for USP34 actions on osteogenesis by performing RNA-Seq analysis. Human MSCs were treated with USP34 or control siRNAs and cultured in osteogenic induction medium for 2 days prior to RNA isolation. Depletion of USP34 from human MSCs increased the expression of 508 genes and decreased the expression of 391 genes (Fig 4A). Notably, a KEGG pathway analysis indicated that USP34 primarily affected the expression of genes associated with TGF-β/BMP signaling pathway (Fig 4B). The well-known target genes of BMP2, including *SP7*, *RUNX2*, *ID1*, *ID2*, and *DLX5*, were significantly downregulated (Fig 4C).

To verify that USP34 is essential for the activation of BMP2 signaling, we then performed a BRE luciferase assay. The BRE-Luc construct used is derived from the promoter of *Id1* gene and contains the most sensitive BMP-responsive elements (Korchynskyi & ten Dijke, 2002; Logeart-Avramoglou *et al*, 2006). We observed that knockdown of *USP34* in 293T cells markedly restricted BMP2-induced responses (Fig 4D). As BMP2 induces the expression of SP7, a master transcriptional factor for osteogenic differentiation, we examined whether this induction requires USP34. Both Western blot and quantitative RT–PCR revealed that deletion of Usp34 from mouse MSCs significantly blunted the expression of Sp7 (Fig 4E and F). MSCs obtained from *Prx1-Cre;Usp34$^{f/f}$* mice also showed decreased ALP activity and calcium mineralization after prolonged BMP2 treatment (Fig 4G–I).

Next, we investigated the *in vivo* function of USP34 in BMP2-induced bone formation by performing calvarial injection experiments. Prx1-Cre recombines in progenitors not only from long bone, but also in those from calvaria (Elefteriou & Yang, 2011; Xiong *et al*, 2011; Ouyang *et al*, 2014). Subcutaneous injection of BMP2 onto the calvaria induces the local recruitment and differentiation of cranial mesenchymal cells into osteoblasts, resulting in the *de novo* formation of cancellous bone (Mundy *et al*, 1999; Addison *et al*, 2014). In comparison with their control littermates, *Prx1-Cre;Usp34$^{f/f}$* mice were markedly less responsive to BMP2 injection, with a nearly 50% reduction in the volume of newly formed bone on the calvaria (Fig 4J and K). Vehicle injections did not induce any bone formation (Fig 4J and K). Histological analysis also revealed that the newly formed bone in *Prx1-Cre;Usp34$^{f/f}$* mice had larger bone marrow spaces and lower bone volume versus total volume (BV/TV) as compared to those of controls (Fig 4L and M).

Finally, we performed calvarial organ culture to assess the role of Usp34 in BMP2 signaling further up. As expected, BMP2 induced sub-periosteal bone formation (Fig 4N and O; light red, in contrast to the red original bone). However, the bone formation in *Prx1-Cre;Usp34$^{f/f}$* calvariae was significantly less than that observed in *Usp34$^{f/f}$* controls (Fig 4N and O). These data demonstrate that *Usp34* deletion within mesenchymal cells blunts their responses to BMP2.

### Deletion of *Usp34* in MSCs impairs bone regeneration

Considering the indispensability of BMP2 activity in initiating fracture healing (Tsuji *et al*, 2006), we subsequently carried out mid-diaphyseal femoral fractures to *Prx1-Cre;Usp34$^{f/f}$* and control mice to evaluate the effect of Usp34 on bone healing. Three weeks after the fracture, microCT analysis showed that healing proceeded much more slowly in *Prx1-Cre;Usp34$^{f/f}$* mice as compared to control mice (Fig 5A). There is a significant decrease in trabecular BV/TV in the callus of *Prx1-Cre;Usp34$^{f/f}$* mice (Fig 5B), along with diminished Tb.N and Tb.Th, as well as elevated trabecular separation (Fig 5C–E). Histomorphometric analysis confirmed that the mineralization in callus bone at the fracture site was significantly lower in *Prx1-Cre;Usp34$^{f/f}$* mice (Fig 5F and H). In contrast to the controls, *Usp34*-deficient mice failed to achieve a comparable bone healing at the fracture site, with a large amount of callus cartilage still remained (Fig 5G and I).

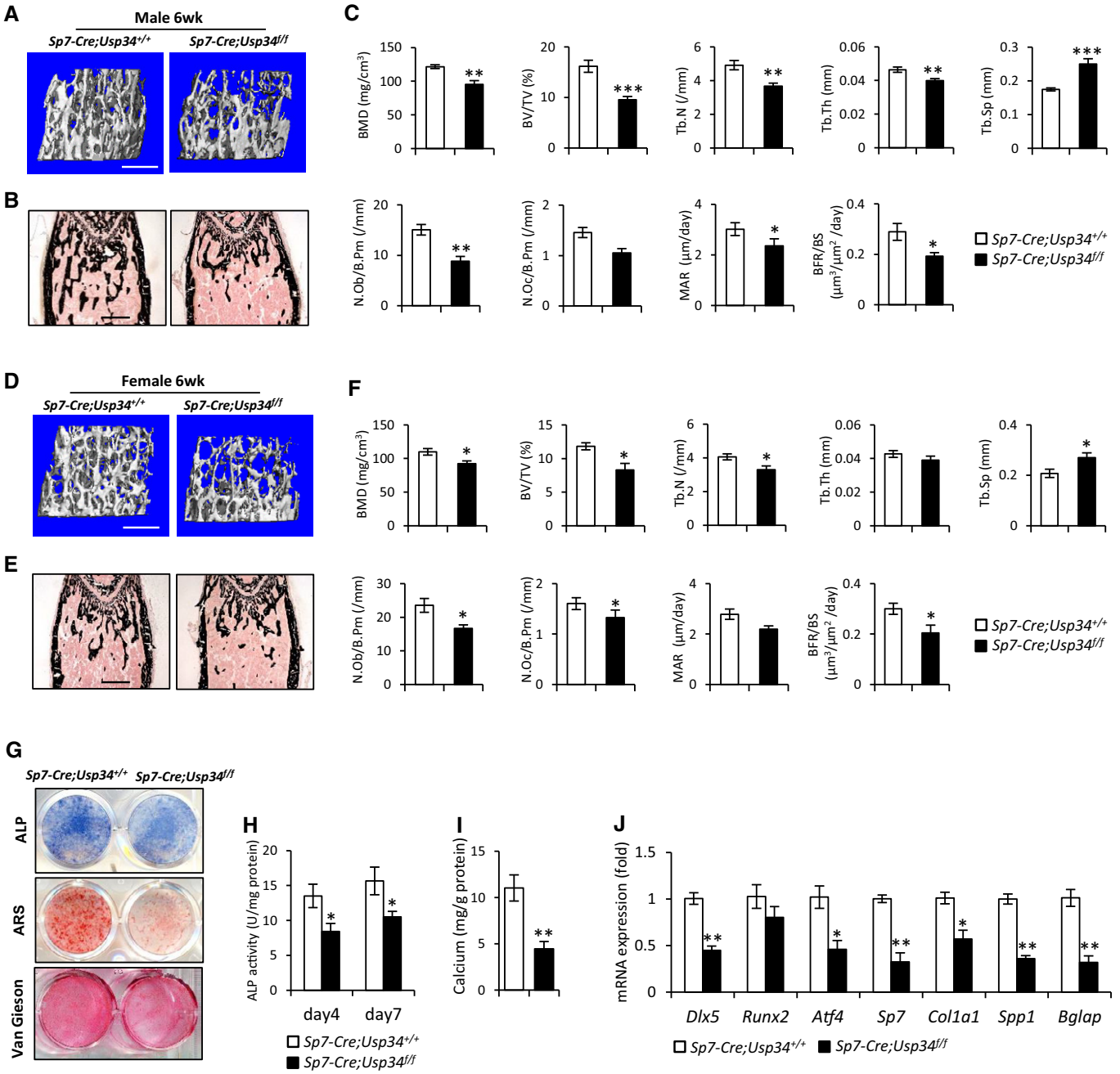


**Figure 3. Conditional deletion of *Usp34* in pre-osteoblasts impairs bone formation.**

A Representative microCT images of trabecular bone from the femoral metaphysis of male *Sp7-Cre;Usp34$^{f/f}$* and littermate control mice. Scale bar, 500 μm.

B, C Von Kossa staining and histomorphometric analyses of male femurs. Scale bar, 500 μm. Results are shown as mean ± SEM; $n = 8$; $^{*}P < 0.05$, $^{**}P < 0.01$, and $^{***}P < 0.001$ by *t*-test.

D Representative microCT images of trabecular bone from the femoral metaphysis of female *Sp7-Cre;Usp34$^{f/f}$* and littermate control mice. Scale bar, 500 μm.

E, F Von Kossa staining and histomorphometric analyses of female femurs. Scale bar, 500 μm. Results are shown as mean ± SEM; $n = 8$; $^{*}P < 0.05$ by *t*-test.

G Representative images of ALP, ARS and Van Gieson's staining of MSCs obtained from *Sp7-Cre;Usp34$^{f/f}$* and littermate control mice.

H, I Quantitative analyses of the ALP activity and calcium mineralization. Results are shown as mean ± SEM; $n = 6$; $^{*}P < 0.05$ and $^{**}P < 0.01$ by *t*-test.

J Quantitative RT–PCR analyses of the transcription of osteogenic markers. Cells were differentiated in osteogenic medium for 5 days. Results are shown as mean ± SEM; $n = 3$; $^{*}P < 0.05$ and $^{**}P < 0.01$ by *t*-test.

For further validation, we surgically created skeletal defects by drilling holes in femoral cortical bone to examine the inhibitory effect of *Usp34* deficiency on bone regeneration. MicroCT and histological analyses consistently showed that the cortical gaps in *Usp34$^{f/f}$* control mice were almost completely bridged after 2 weeks, while those in *Prx1-Cre;Usp34$^{f/f}$* were only partially filled (Fig 5J

 

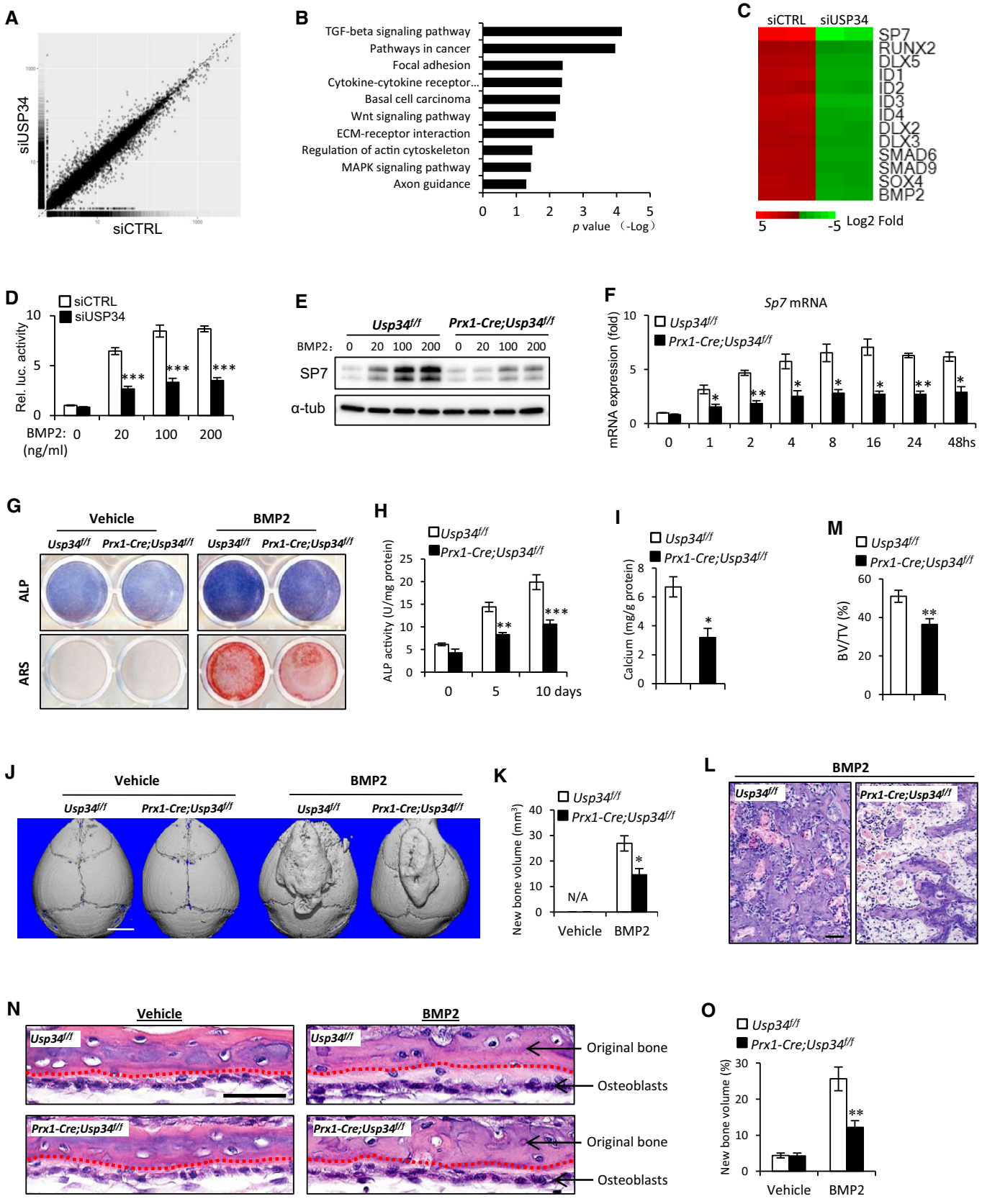
A
siUSP34
siCTRL
B
TGF-beta signaling pathway
Pathways in cancer
Focal adhesion
Cytokine-cytokine receptor...
Basal cell carcinoma
Wnt signaling pathway
ECM-receptor interaction
Regulation of actin cytoskeleton
MAPK signaling pathway
Axon guidance
0 1 2 3 4 5
p value （-Log）
C
siCTRL siUSP34
SP7
RUNX2
DLX5
ID1
ID2
ID3
ID4
DLX2
DLX3
SMAD6
SMAD9
SOX4
BMP2
5 -5 Log2 Fold
D
siCTRL
siUSP34
Rel. luc. activity
BMP2: 0 20 100 200
(ng/ml)
E
Usp34f/f Prx1-Cre;Usp34f/f
BMP2: 0 20 100 200 0 20 100 200
SP7
α-tub
F
Sp7 mRNA
Usp34f/f
Prx1-Cre;Usp34f/f
mRNA expression (fold)
0 1 2 4 8 16 24 48hs
G
Vehicle
BMP2
Usp34f/f Prx1-Cre;Usp34f/f Usp34f/f Prx1-Cre;Usp34f/f
ALP
ARS
H
Usp34f/f
Prx1-Cre;Usp34f/f
ALP activity (U/mg protein)
0 5 10 days
I
Usp34f/f
Prx1-Cre;Usp34f/f
Calcium (mg/g protein)
M
Usp34f/f
Prx1-Cre;Usp34f/f
BV/TV (%)
J
Vehicle
BMP2
Usp34f/f Prx1-Cre;Usp34f/f Usp34f/f Prx1-Cre;Usp34f/f
K
Usp34f/f
Prx1-Cre;Usp34f/f
New bone volume (mm3)
N/A
Vehicle BMP2
L
BMP2
Usp34f/f
Prx1-Cre;Usp34f/f
N
Vehicle
BMP2
Usp34f/f
Prx1-Cre;Usp34f/f
Original bone
Osteoblasts
O
Usp34f/f
Prx1-Cre;Usp34f/f
New bone volume (%)
Vehicle BMP2

**Figure 4.**

**Figure 4. Loss of USP34 blunts BMP2-induced responses.**

A Scatter plot of RNA-seq expression analysis. A total of 508 genes were upregulated and 391 genes were downregulated. Human MSCs were transfected with USP34 or control siRNAs and cultured in osteogenic medium for 2 days. Two biological replicates per group.

B KEGG pathway analysis indicated the altered function of TGF-β/BMP signaling pathway.

C Heatmap of representative genes associated with BMP2 signaling pathway.

D Relative activity of BRE luciferase assay. 293T cells were depleted with serum overnight followed by a treatment with BMP2 for 6 h. Results are shown as mean ± SEM; $n = 3$. ***$P < 0.001$ by $t$-test.

E Immunoblot analysis of BMP2-induced Sp7 expression. *Prx1-Cre;Usp34$^{f/f}$* and *Usp34$^{f/f}$* control MSCs were starved overnight and then stimulated with 100 ng/ml BMP2 for 24 h.

F Quantitative RT–PCR analysis of BMP2-induced *Sp7* transcription. Cells were depleted from serum overnight before BMP2 stimulation. Results are shown as mean ± SEM; $n = 3$; *$P < 0.05$ and **$P < 0.01$ by $t$-test.

G Representative images of ALP and ARS staining. MSCs were cultured with normal medium supplemented with 100 ng/ml BMP2 for 10 and 21 days, respectively.

H, I Quantitative analyses of the ALP activity ($n = 4$) and calcium mineralization ($n = 5$). Results are shown as mean ± SEM; *$P < 0.05$, **$P < 0.01$, and ***$P < 0.001$ by $t$-test.

J, K Representative microCT images and quantification of newly formed bone in response to BMP2. Results are shown as mean ± SEM; $n = 8$. *$P < 0.05$ by $t$-test. Scale bar, 2,500 μm.

L H&E staining of BMP2-induced newly formed bone. Scale bar, 50 μm.

M Quantitative analysis of bone volume versus total tissue volume (BV/TV). Results are shown as mean ± SEM; $n = 8$; **$P < 0.01$ by $t$-test.

N H&E staining of calvarial organ cultures stimulated with or without 100 ng/ml BMP2. Red dotted lines indicate the interface between original and newly formed bone. Scale bar, 50 μm.

O Quantitative analysis of newly formed bone volume versus original bone volume (%). Results are shown as mean ± SEM; $n = 8$; **$P < 0.01$ by $t$-test.

Source data are available online for this figure.

and K). Additionally, the BMD and BV/TV of the mineralized callus of *Prx1-Cre;Usp34$^{f/f}$* mice were significantly lower than their controls (Fig 5L and M). The osteoblast surfaces (Ob.S/BS) were also diminished (Fig 5N).

### USP34 stabilizes Smad1 and RUNX2

BMP2 triggers osteogenic differentiation mainly through activation of Smad1/5/8 to induce the expression of downstream transcriptional factors such as DLX5, RUNX2, and SP7 (Rahman *et al*, 2015; Salazar *et al*, 2016; Wu *et al*, 2016). To uncover the substrates of USP34, we first ectopically expressed FLAG-tagged Smad1 in 293T cells and revealed that it could be detected in USP34 immunoprecipitates (Fig 6A). And knockdown of *USP34* significantly reduced the protein levels of FLAG-Smad1 (Fig 6B), while increased its ubiquitination (Fig 6C), indicating a key role for USP34-dependent deubiquitination of Smad1. We then determined whether USP34 in fact regulates the stability of the Smad1 protein by observing FLAG-Smad1 protein levels in the presence of cycloheximide (CHX), an inhibitor of protein translation. Depleting USP34 using siRNA resulted in much faster degradation of FLAG-Smad1 protein (Fig 6D).

In addition, we discovered that USP34 could physically interact with RUNX2, a downstream factor of Smad1 (Fig 6E and F). And *Prx1-Cre;Usp34$^{f/f}$* MSCs showed significantly increased RUNX2 ubiquitination compared to *Usp34$^{f/f}$* controls (Fig 6G). We then evaluated the stability of RUNX2 protein in *Prx1-Cre;Usp34$^{f/f}$* MSCs and observed a more prominent degradation compared to the *Usp34$^{f/f}$* controls (Fig 6H). These results indicate that USP34 also acts as a *bona fide* deubiquitinase that stabilizes RUNX2.

### Combined overexpression of Smad1 and Runx2 rescues the osteogenic potential of *Usp34*-deficient MSCs

To further establish that decreased Smad1 and RUNX2 contributed to inhibited osteogenesis of *Usp34*-deficient MSCs, we transduced *Prx1-Cre;Usp34$^{f/f}$* MSCs with *Smad1* adenoviruses (Ad-Smad1), *Runx2* adenoviruses (Ad-Runx2), or a combination. The combination of Ad-Smad1 and Ad-Runx2 successfully restored the weak ALP activity and calcium mineralization in *Prx1-Cre;Usp34$^{f/f}$* MSCs (Fig 6I–K), while single restoration of either Smad1 or Runx2 was insufficient to reverse the osteogenic incompetence.

In addition, we subcutaneously implanted cells that overexpressed *Smad1* or/and *Runx2* with β-TCP carriers into immunocompromised mice to testify their ability to ectopically form bone tissue. In consistent with *in vitro* findings, histological analysis confirmed that only concurrent overexpression of *Smad1* and *Runx2* could fully rescue the compromised bone formation of *Prx1-Cre;Usp34$^{f/f}$* cells (Fig 6L and M), demonstrating that both Smad1 and RUNX2 are critical substrates for USP34's control in osteogenic differentiation.

### Depletion of *Smurf1* restores the BMP2-induced responses and osteogenic potential of *Usp34*-deficient MSCs

Since Smurf1, an E3 ubiquitin ligase, regulates BMP2 signaling through directly interacting and degrading Smad1 and RUNX2 (Zhu *et al*, 1999; Zhao *et al*, 2003), we hypothesized that it couples USP34 to balance the BMP2 signaling. To this end, we knocked down both of them in 293T cells and performed BRE luciferase assay. Interestingly, knockdown of *Smurf1* in *Usp34*-depleted cells successfully restored BMP2-induced luciferase activity (Fig 7A). Considering the master role of SP7 in osteogenesis, we measured the expression of Sp7 to assess the extent of recovery in BMP2-induced response of *Prx1-Cre;Usp34$^{f/f}$* MSCs upon depletion of *Smurf1*. Both Western blot and quantitative RT–PCR showed that the restricted expression of Sp7 in *Prx1-Cre;Usp34$^{f/f}$* MSCs was rescued by *Smurf1* siRNA (Fig 7B and C). Moreover, depletion of *Smurf1* restored the BMP2-induced ALP activity and calcium mineralization in *Prx1-Cre;Usp34$^{f/f}$* MSCs (Fig 7D and E).

Finally, we sought to investigate whether depletion of Smurf1 is sufficient to recover the osteogenic potential of *Prx1-Cre;Usp34$^{f/f}$*

 

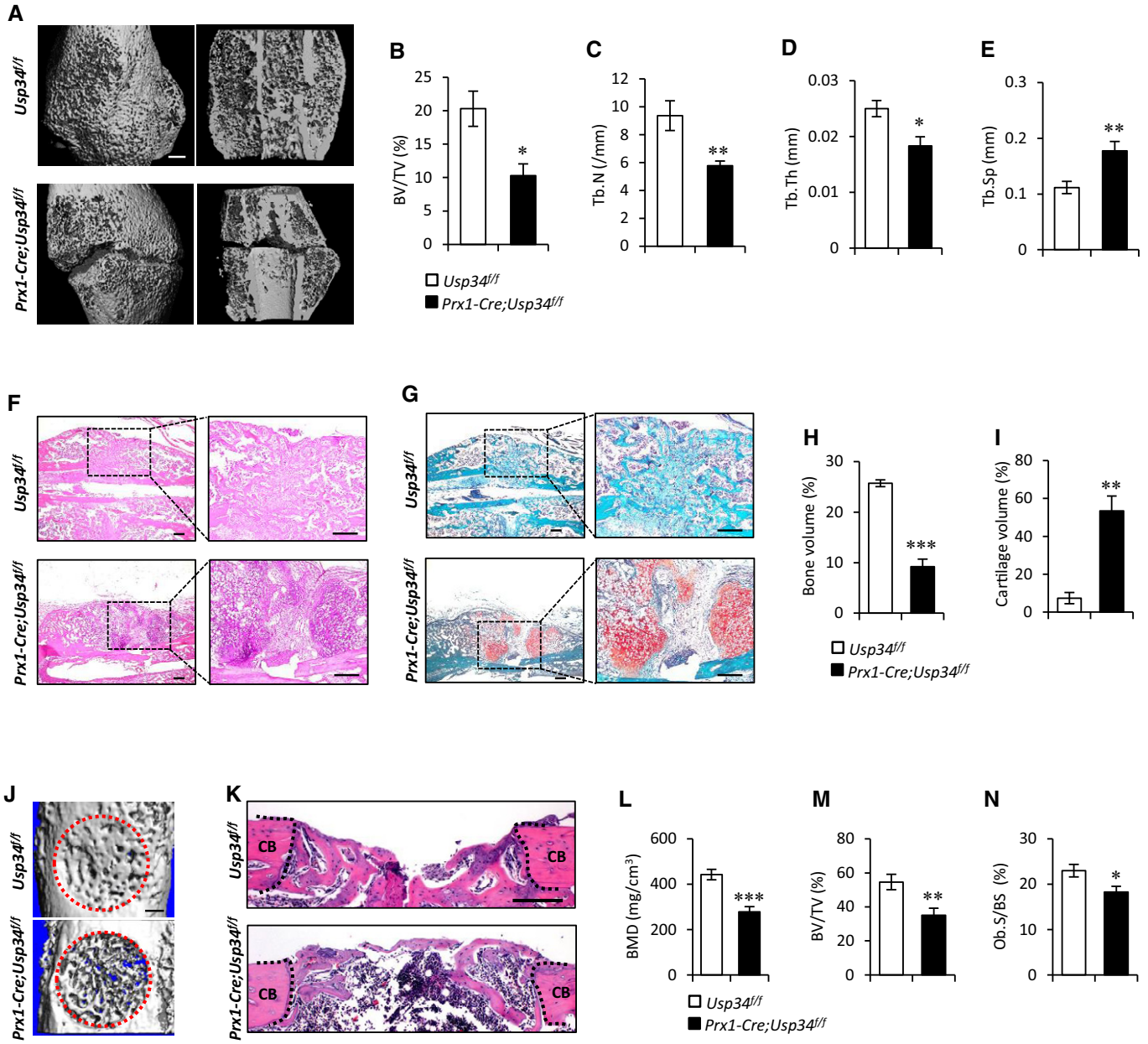


**Figure 5. Deletion of USP34 in MSCs impairs bone regeneration.**

A Representative microCT 3D reconstruction and cut-plane images of the fracture site 3 weeks after bone fracture. Scale bar, 500 μm.

B–E MicroCT analyses of trabecular bone volume (BV/TV), trabecular number (Tb.N), trabecular thickness (Tb.Th), and trabecular separation (Tb.Sp). Results are shown as mean ± SEM; $n = 8$; *$P < 0.05$ and **$P < 0.01$ by $t$-test.

F, G Representative images of H&E (F) and Safranin O (G) staining of the fracture callus 3 weeks after bone fracture. Scale bar, 200 μm.

H, I Quantification of the mineralized bone callus (H) and cartilage callus (I) in the fracture site. Results are shown as mean ± SEM; $n = 8$; **$P < 0.01$ and ***$P < 0.001$ by $t$-test.

J Representative microCT images of femoral cortical bone defects in *Prx1-Cre;Usp34*$^{f/f}$ and *Usp34*$^{f/f}$ control mice. The red dotted lines indicate the position of the original defect margin. Scale bar, 500 μm.

K H&E staining of femoral cortical bone defects. The black dotted lines indicate the position of the original defect margin. CB, cortical bone. Scale bar, 200 μm.

L–N Bone mineral density (BMD), bone volume (BV/TV), and osteoblast surface (Ob.S/BS) of the regenerated bone in femoral cortical gaps. Results are shown as mean ± SEM; $n = 8$; *$P < 0.05$, **$P < 0.01$, and ***$P < 0.001$ by $t$-test.

MSCs *in vitro*. After culturing with osteogenic induction medium for 5 and 10 days, respectively, the ALP activity and calcium mineralization of *Prx1-Cre;Usp34*$^{f/f}$ + siSmurf1 MSCs were comparable to those of *Usp34*$^{f/f}$ controls (Fig 7F–H). Besides, the expression of osteogenic markers, such as *Dlx5*, *Runx2*, *Sp7*, and *Bglap*, was also recovered and no longer inhibited after the treatment (Fig 7I and J),

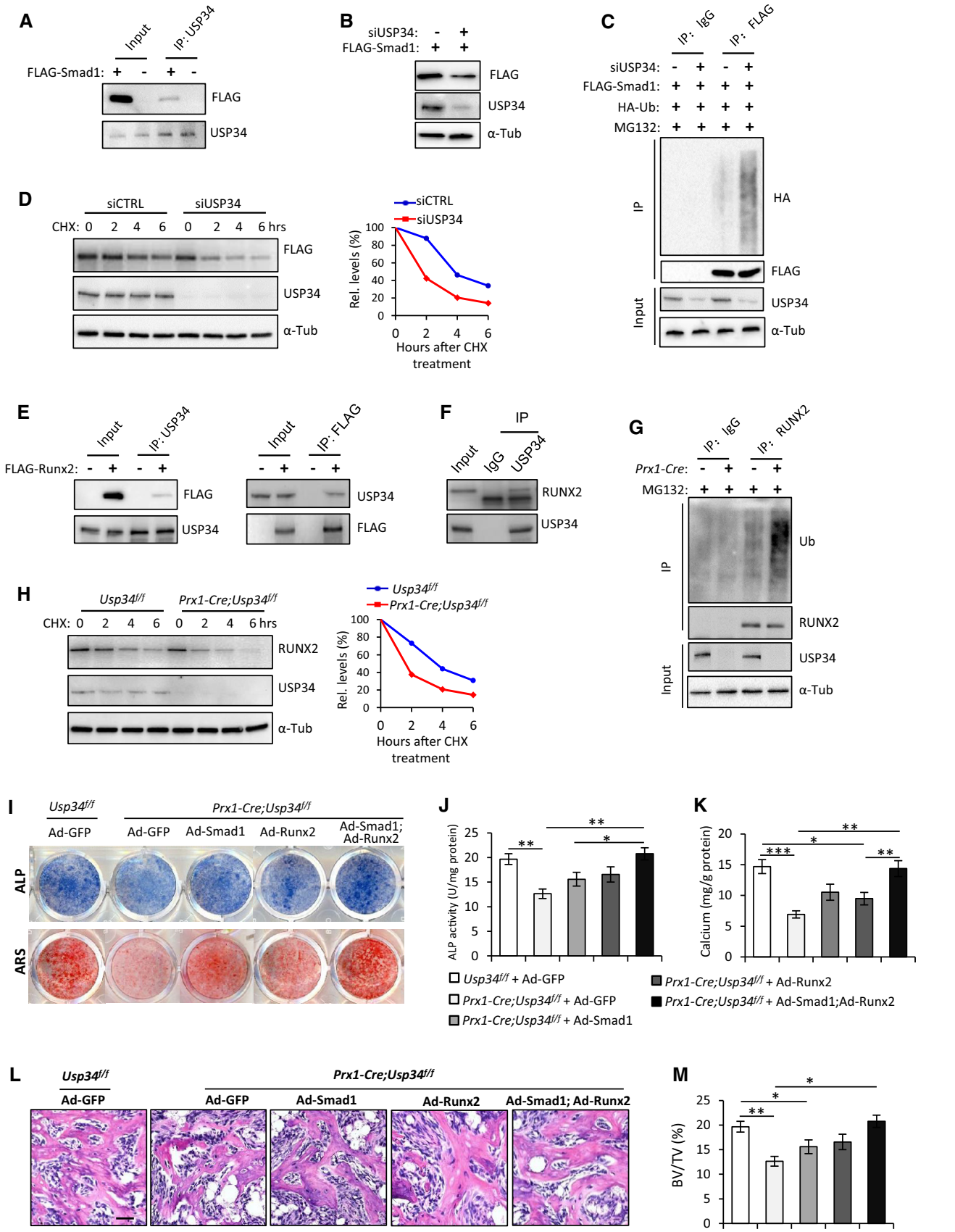


**Figure 6.**

 

**Figure 6. USP34 deubiquitinates and stabilizes Smad1 and RUNX2.**

A Co-immunoprecipitation of USP34 with ectopically expressed FLAG-tagged Smad1 in 293T cells.

B Immunoblot analysis showing decreased FLAG-Smad1 after USP34 knockdown.

C Immunoblot of Smad1-linked polyUb. 293T cells were co-transfected with FLAG-Smad1 overexpression plasmid and USP34 siRNA, and treated with 10 μM MG132 for 4 h before collection.

D Immunoblot analysis of the degradation of FLAG-Smad1 protein. 293T cells were co-transfected with FLAG-Smad1 overexpression plasmid and USP34 siRNA, and treated with 50 μg/ml cycloheximide (CHX) before collection at designated time points. Right: relative quantification of FLAG-Smad1 protein levels at different time points.

E Co-immunoprecipitation of USP34 with ectopically expressed FLAG-tagged RUNX2 in 293T cells.

F Co-immunoprecipitation of USP34 with endogenous RUNX2 in mouse MSCs.

G Immunoblot of RUNX2-linked polyUb. Differentiated mouse MSCs were treated with 10 μM MG132 for 4 h before collection. *Prx1-Cre*(+) indicates MSCs isolated from *Prx1-Cre;Usp34*$^{f/f}$ mice, and *Prx1-Cre*(−) indicates those from *Usp34*$^{f/f}$ control mice.

H Immunoblot analysis of the degradation of endogenous RUNX2 protein in MSCs. *Prx1-Cre;Usp34*$^{f/f}$ and *Usp34*$^{f/f}$ control MSCs were stimulated with BMP2, treated with 50 μg/ml CHX, and collected at designated time points. Right: relative quantification of RUNX2 protein levels at different time points.

I Representative images of ALP and ARS staining. *Usp34*$^{f/f}$ and *Prx1-Cre;Usp34*$^{f/f}$ MSCs were transduced with GFP, Smad1, Runx2, or Smad1 + Runx2 adenoviruses and then cultured in osteogenic medium for 5 and 10 days, respectively.

J, K Quantitative analyses of the ALP activity and calcium mineralization. Results are shown as mean ± SEM; $n = 8$; $^{*}P < 0.05$, $^{**}P < 0.01$, and $^{***}P < 0.001$ by ANOVA with Tukey's *post hoc* test.

L, M H&E staining and quantitative analysis of MSC-mediated ectopic bone formation. Scale bar, 50 μm. Results are shown as mean ± SEM; $n = 8$; $^{*}P < 0.05$ and $^{**}P < 0.01$ by ANOVA with Tukey's *post hoc* test.

Source data are available online for this figure.

indicating that USP34 sequesters Smurf1 to promote osteogenic differentiation.

## Discussion

The proper osteogenic differentiation is essential for bone homeostasis. Here, we have profiled the expression of 54 USPs in human MSCs after osteogenic induction and identified USP34 as a previously unknown regulator of osteogenesis. Our *in vitro* and *in vivo* data demonstrate that USP34 is essential for the osteogenic differentiation and bone formation. Although the expression of USP13, USP18, USP21, and USP53 was also increased after osteogenic induction, knockdown of these genes did not have a significant effect. Previous reports show that USP1 and USP6 maintain the stem-cell-like properties and inhibit the osteogenic commitment in osseous tumors (Ye *et al*, 2010; Williams *et al*, 2011). A recent study also suggests that USP4 antagonizes osteoblast differentiation *in vitro* through deubiquitination of Dishevelled (Zhou *et al*, 2016). These data, together with our findings, indicate that USPs may play a pivotal role in maintaining skeletal homeostasis.

In this study, we show that loss of USP34 blunts BMP2 signaling, which is indispensable for osteogenesis and bone fracture healing. It triggers osteogenic commitment of MSCs mainly through activation of Smad1/5/8 that subsequently induces the expression of transcriptional factors, such as RUNX2, MSX1, and DLX5 (Rahman *et al*, 2015; Salazar *et al*, 2016; Wu *et al*, 2016). To elucidate the underlying molecular mechanism, we first identified Smad1, the critical element of BMP2 signaling, as a substrate of USP34. This is consistent with the previous study which shows that USP34 interacted with Smad1/5/8 and that depletion of USP34 in HeLa cells by siRNA reduced the level of total Smad1/5/8 (Cheng *et al*, 2012). We also discovered that USP34 targeted the downstream transcriptional factor RUNX2. Both mRNA and protein levels of RUNX2 were decreased in the *Usp34*-deficient MSCs, indicating that USP34 regulates the expression of RUNX2 not only through Smad-dependent transcriptional activation, but also through post-transcriptional ubiquitination. Our rescue experiments also showed that only combined overexpression, but not single overexpression of *Smad1* or *Runx2*, was able to fully recover osteogenic potential of Usp34-deficient MSCs, confirming USP34 targets on both Smad1 and Runx2.

**Figure 7. Depletion of Smurf1 restores the BMP2-induced responses and osteogenic potential of *Usp34*-deficient MSCs.**

A Relative activity of BRE luciferase assay. 293T cells were depleted with serum overnight followed by a treatment with BMP2 for 6 h. Results are shown as mean ± SEM; $n = 3$. $^{*}P < 0.05$ by ANOVA with Tukey's *post hoc* test.

B Immunoblot analysis of BMP2-induced Sp7 expression. *Prx1-Cre;Usp34*$^{f/f}$ MSCs were treated with Smurf1 or control siRNAs, starved overnight, and then stimulated with 100 ng/ml BMP2 for 24 h.

C Quantitative RT–PCR analysis of BMP2-induced *Sp7* transcription. *Prx1-Cre;Usp34*$^{f/f}$ MSCs were treated with Smurf1 or control siRNAs, and depleted from serum overnight before BMP2 stimulation. Results are shown as mean ± SEM; $n = 3$; $^{*}P < 0.05$ and $^{**}P < 0.01$ by ANOVA with Tukey's *post hoc* test.

D ALP staining and quantitative measurement of ALP activity. MSCs were cultured with normal medium supplemented with 100 ng/ml BMP2 for 5 days. Results are shown as mean ± SEM; $n = 8$; $^{**}P < 0.01$ by ANOVA with Tukey's *post hoc* test.

E Representative images of ARS staining and quantification. Cells were cultured with normal medium supplemented with 100 ng/ml BMP2 for 14 days. Results are shown as mean ± SEM; $n = 8$; $^{*}P < 0.05$ and $^{**}P < 0.01$ by ANOVA with Tukey's *post hoc* test.

F Representative images of ALP and ARS staining. Mouse MSCs were treated with Smurf1 or control siRNAs, and cultured in osteogenic medium for 5 and 10 days, respectively.

G, H Quantitative analyses of the ALP activity and calcium mineralization. Results are shown as mean ± SEM; $n = 8$; $^{*}P < 0.05$, $^{**}P < 0.01$, and $^{***}P < 0.001$ by ANOVA with Tukey's *post hoc* test.

I, J Quantitative RT–PCR and Western blot analyses of the expression of osteogenic markers. Cells were treated with Smurf1 or control siRNAs, and cultured in osteogenic medium for 5 days. Results are shown as mean ± SEM; $n = 3$; $^{*}P < 0.05$, $^{**}P < 0.01$, and $^{***}P < 0.001$ by ANOVA with Tukey's *post hoc* test.

Source data are available online for this figure.

The previous study reported that USP34 regulates axin stability and Wnt/β-catenin signaling (Lui *et al*, 2011). Our KEGG pathway analysis of the RNA-Seq data also suggests that Wnt signaling may be associated with USP34 activity ($P$ = 0.007, Fig 4B). To confirm this observation, we isolated femoral bone samples from 12-week-old *Prx1-Cre;Usp34*$^{f/f}$ and *Usp34*$^{f/f}$ mice, and compared the mRNA levels of *Axin1*, *Axin2*, *Dkk1*, and *β-catenin*. However, no significant difference was identified (Appendix Fig S6). The potential role of Wnt signaling in USP34-mediated bone formation needs further investigation.

Here, we report USP34 as the first documented deubiquitinase for RUNX2, a runt domain family protein that is essential for the commitment of mesenchymal cells to the osteoblast lineage. Both intramembranous and endochondral ossification are absent in

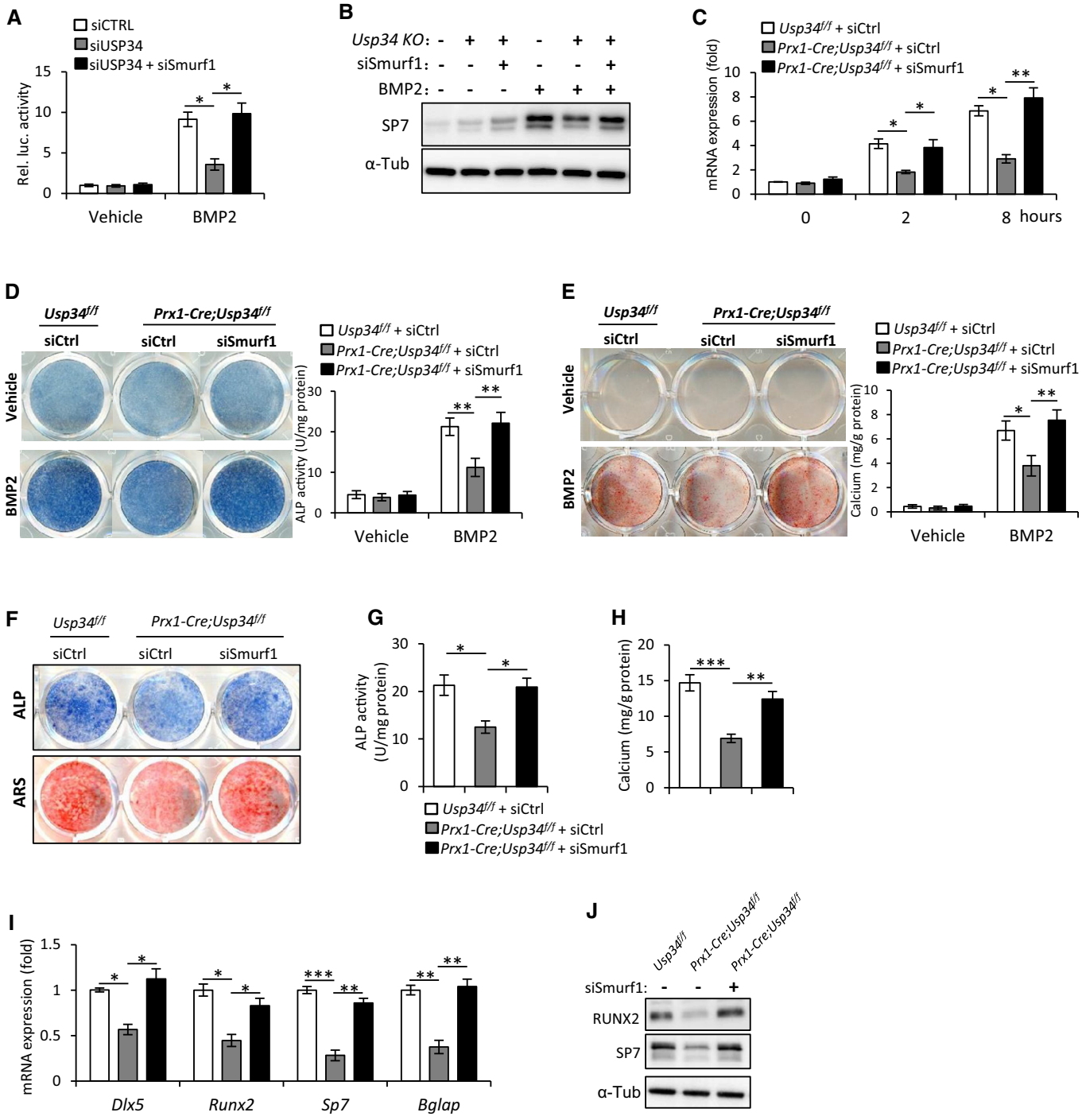


**Figure 7.**

*Runx2* knockout mice (Komori *et al*, 1997; Otto *et al*, 1997). Previous studies have shown that RUNX2 could be degraded by ubiquitin ligases, such as Smurf1, WWP1, and CHIP (Zhao *et al*, 2003, 2004; Jones *et al*, 2006; Li *et al*, 2008; Shu *et al*, 2013). However, its deubiquitinase has not been discovered before.

Smurf1 is the first E3 ligase identified for RUNX2 ubiquitination (Zhao *et al*, 2003, 2004). It also mediates the degradation of Smad1 (Zhu *et al*, 1999). Smurf1-deficient mice exhibit enhanced osteoblast activities and an age-dependent increase in bone mass (Zhao *et al*, 2004; Yamashita *et al*, 2005). This phenotype is opposite to that we observed in *Prx1-Cre;Usp34*$^{f/f}$ and *Sp7-Cre;Usp34*$^{f/f}$ mice. Interestingly, we observed that depletion of Smurf1 is able to fully restore the BMP2-induced responses and osteogenic potential of *Usp34*-deficient MSCs, suggesting USP34 couples Smurf1 to orchestrate the BMP2 signaling.

The data in this study were based on loss-of-function experiments. We attempted overexpression of USP34 in MSCs and MC3T3-E1 cells, but were unsuccessful due to technical difficulty. The entire ORF of *USP34* is over 10 kb, which is too large. We have tried to activate transcription of endogenous USP34 using a CRISPR/Cas9 lentiviral activation particles (Santa Cruz). Unfortunately, it turned out that the efficiency for *USP34* in MSCs was not sufficient. We believe the evidence presented in this study is strong but could be improved with the performance of such experiments.

In summary, we show that expression of USP34 in human MSCs increases after osteogenic induction and depletion of USP34 inhibits osteogenic differentiation. Specific deletion of *Usp34* from MSCs or pre-osteoblasts results in low bone mass and decreased osteoblast function in mice. Moreover, loss of *Usp34* blunts BMP2-induced responses and impairs bone regeneration. Mechanically, USP34 stabilizes both Smad1 and RUNX2. Our data demonstrate that USP34 is a previously unknown regulator of osteogenic differentiation and bone formation.

## Materials and Methods

### Reagents

Recombinant human BMP2 (#120-02C) and Wnt3a (#315-20) were purchased from PeproTech (Rocky Hill, NJ). The antibodies used are as follows: rabbit anti-USP13 (A302-762A, Bethyl), rabbit anti-USP18 (sc-98431, Santa Cruz), goat anti-USP21 (sc-79305, Santa Cruz), rabbit anti-USP34 (A300-824A, Bethyl), rabbit anti-USP53 (HPA035844, Sigma), rabbit anti-DLX5 (HPA005670, Sigma), rabbit anti-RUNX2 (Ab23981, Abcam), rabbit anti-SP7 (ab22552, Abcam), mouse anti-FLAG-M2 (F1804, Sigma), rabbit anti-FLAG (F7425, Sigma), mouse anti-HA (901502, BioLegend), and mouse anti-α-tubulin (sc-32293, Santa Cruz). The construct for HA-Ubiquitin (#17608) was obtained from Addgene (Cambridge, MA). The FLAG-RUNX2 plasmid is a gift from Dr. Weiguo Zou (Institute of Biochemistry and Cell Biology, Shanghai).

### Mice

*Usp34* conditional knockout mice were generated by a CRISPR/Cas9-based approach. Briefly, two sgRNAs were designed with a CRISPR design tool (http://crispr.mit.edu) to target either a region upstream or downstream of the exon 2 (Appendix Table S1). These were then screened for on-target activity using a Universal CRISPR Activity Assay (UCA™, Biocytogen Inc, Beijing). A T7 promoter sequence was added to the Cas9 or sgRNA template by PCR amplification *in vitro*. A circular targeting vector containing exon 2 flanked by two *LoxP* sites and two homology arms was mixed with Cas9 mRNA and sgRNAs and then co-injected into the cytoplasm of one-cell stage fertilized C57BL6/J eggs. The injected zygotes were transferred into oviducts of Kunming pseudopregnant females to generate F0 mice. F0 mice with expected genotype confirmed by tail genomic DNA PCR and sequencing were mated with C57BL6/J mice to establish germline-transmitted F1 founders. F1 founders were genotyped by tail genomic PCR and DNA sequencing. Southern blot examination was performed to further confirm correct genotype. *Prx1-Cre* mice were purchased from the Jackson Laboratory (Bar Harbor, ME) and mated with *Usp34*$^{f/f}$ mice for at least three generations to generate *Prx1-Cre;Usp34*$^{f/f}$ conditional knockout mice. Genotypes were determined by PCR amplification of purified tail genomic DNA. Primers are listed in Appendix Table S1. Female immunocompromised nude mice were purchased from the Experimental Animal Center of Sichuan University. Mice were housed in pathogen-free facilities under a 12-h light and 12-h dark cycle. All protocols were approved by the Subcommittee on Research and Animal Care (SRAC) of Sichuan University.

### Cell culture

Human bone marrow-derived mesenchymal stem cells (MSCs) were obtained from ATCC. We cultured the cells in α-MEM (Gibco) supplemented with 10% fetal bovine serum (FBS, Gibco), plus 100 units/ml penicillin and 100 μg/ml streptomycin (Gibco) at 37°C with a humidified atmosphere of 5% $CO_2$. Primary mouse MSCs were isolated from 6-week-old mice by flushing the bone marrow of tibiae and femurs (Song *et al*, 2012). Primary osteoblasts were isolated from the calvariae of 3-day-old mice as described previously (Yuan *et al*, 2012). To induce osteogenic differentiation, MSCs were seeded in 6-well or 24-well plates. After confluence, cells were treated with osteogenic medium containing 50 μM ascorbic acid, 10 mM β-glycerophosphate, and 10 nM dexamethasone (all from Sigma).

### Isolation of *Prx1-Cre;tdTomato*$^{+}$ cells

Bone marrow was flushed out from femurs of young (3-month-old) and aged (18-month-old) *Prx1-Cre;tdTomato* mice and then treated with red blood cell lysis buffer (Santa Cruz) for 10 min at room temperature. After rinsing with cold PBS, the nucleated marrow cells were incubated with APC-conjugated CD45 antibody (BioLegend) and APC-conjugated CD11b antibody (BioLegend) and were subjected to flow cytometry (Becton-Dickinson LSRII). The cell gating was based on comparison with negative control and single-stained controls.

### siRNA knockdown, lentivirus-mediated shRNA knockdown, and adenovirus-mediated overexpression of MSCs

All targeted and control small interfering RNAs (siRNAs) were purchased from Santa Cruz (Dallas, Texas). Each siRNA consists of pools with three to five target-specific 19- to 25-nucleotide siRNAs

designed to knock down target gene expression. For siRNA-mediated knockdown, human MSCs or 293T cells were transfected using Lipofectamine RNAimax (Invitrogen) following the manufacturer's instructions. Knockdown efficiencies were examined by quantitative RT–PCR and Western blot 48 h after the start of transfection. For shRNA-mediated knockdown, the USP34 shRNA expression lentiviruses were purchased from GeneCopoeia (Guangzhou, China). Stably transfected clones were selected with puromycin (Invitrogen) for about 7 days. For overexpression of Smad1 and Runx2, the adenovirus particles expressing mouse Smad1, Runx2, or GFP (control) were obtained from Cyagen (Guangzhou, China).

#### Quantitative RT–PCR and RNA-Seq

We isolated the total RNA using an RNeasy mini kit (Qiagen). cDNA was prepared from 2 μg RNA using a QuantiTect reverse transcription kit (Qiagen) and analyzed with SYBR Premix Ex Taq (Takara, Dalian, China) in ABI7500 real-time PCR system (Applied Biosystems, Foster City, CA). Relative expression was calculated using a $2^{-\Delta\Delta C_t}$ method by normalizing with *Gapdh* housekeeping gene expression and presented as fold increase relative to control.

For RNA-Seq, libraries were prepared using the Illumina TrueSeq mRNA sample preparation kit according to the manufacturer's instruction and single-end sequenced on an Illumina HiSeq 3000 machine. The reads were aligned to hg19 genome using TopHat. The analysis of RNA-seq data was done using Cufflinks with Refseq mRNAs to guide assembly and the cummeRbund package in R (Trapnell *et al*, 2012). Transcripts, which were regulated greater than twofold with significant difference, were used for KEGG pathway analysis.

#### Western blot and co-immunoprecipitation

Cells were lysed in RIPA buffer (Pierce, Rockford, IL) on ice. The samples were heated at 95°C for 5 min in sample buffer containing 2% SDS and 1% 2-mercaptoethanol, separated on 5% or 10% SDS–polyacrylamide gels, and transferred to PVDF membranes by a wet transfer apparatus (Bio-Rad). The membranes were blotted with 5% milk for 1 h and then incubated with primary antibodies overnight, followed by incubation with a horseradish peroxidase-conjugated IgG (Jackson ImmunoResearch, West Grove, PA). The antibody–antigen complexes were visualized with Immobilon reagents (Millipore).

For co-immunoprecipitation, cells or primary mouse MSCs were lysed in CelLytic M buffer (Sigma) supplemented with protease inhibitor cocktail (Roche) for 20 min on ice and centrifuged at 10,000 *g* for 15 min at 4°C. The supernatant was incubated with the indicated antibodies at 4°C overnight, followed by incubation with a 30 μl of Dynabeads protein G (Life Technologies) for additional 1 h. Co-precipitated proteins were washed, eluted with SDS-loading buffer at 95°C for 5 min, and then subjected to Western blot analyses.

#### ALP and mineralization assays

The differentiated cells were fixed with 10% buffered formalin and incubated with 0.1 M Tris buffer (pH 9.3) containing 0.25% naphthol AS-BI phosphate (Sigma) and 0.75% Fast Blue BB (Sigma). ALP activity was also quantified using a commercial kit according to the manufacturer's protocol (Cell Biolabs, San Diego, CA).

The mineralization assay was performed as previously described (Liu *et al*, 2016c). Briefly, cells were cultured in osteogenic medium for 10–14 days, fixed with 10% buffered formalin, and stained with 1% alizarin red S (pH 4.2, Sigma-Aldrich) for 5 min. Mineralized matrix stained with alizarin red were destained with 10% cetylpyridinium chloride in 10 mM sodium phosphate (pH 7.0), and the calcium concentration was determined by absorbance measurements at 562 nm using a standard calcium curve in the same solution.

#### BRE luciferase assay

293T cells seeded in the 24-well plates were transfected with USP34 or control siRNA, together with 100 ng of BRE luciferase (#45126 Addgene) and 50 ng of CMV-beta-galactosidase constructs using Lipofectamine 2000 (Invitrogen). After about 24 h, the cells were depleted with serum overnight followed by a treatment with 100 ng/ml BMP2 for 6 h. The luciferase and β-galactosidase activity of total cell lysates were determined using Luc-Screen and Galacto-Star kits (Applied Biosystems).

#### Xenograft model for MSC-mediated bone formation

Approximately $5 \times 10^6$ cells were mixed with 60 mg of pure phase beta-tricalcium phosphate particles (SynthoGraft, Bicon, Boston, MA), which is a kind of tricalcium phosphate material that exists as crystalline polymorphs beta, and then transplanted subcutaneously under the dorsal surface of immunocompromised beige mice as described (Zhou *et al*, 2017). Six weeks after transplantation, the transplants were collected, fixed with 10% formalin, and decalcified with 10% EDTA. Paraffin sections were fabricated and stained with hematoxylin and eosin.

#### Immunohistochemical staining

The dissected femurs were fixed in 4% polyoxymethylene for 2 days and decalcified in 10% EDTA for 2 weeks before sectioning (5 μm). Slides were subjected to sodium citrate buffer at 99°C for 20 min for antigen retrieval and then incubated with mouse anti-USP34 (1:50, sc-100631, Santa Cruz).

#### MicroCT analysis and bone histomorphometry

The harvested bone tissues were fixed in 10% buffered formalin for 2 days and then stored in 70% ethanol at 4°C before being processed. MicroCT analysis was performed according to recent guidelines (Bouxsein *et al*, 2010) using a μCT 80 microCT system (Scanco Medical, Bassersdorf, Switzerland) with a spatial resolution of 8 μm (55 kV, 114 mA, 500 ms integration time). For the analysis of cortical bone regeneration, the volume of interest (VOI) was defined as a cylindrical area covering the initial bone defect. Bone volume (BV/TV, %) was calculated within the delimited VOI.

Processing of undecalcified bone specimens and cancellous bone histomorphometry was performed as described previously (Yuan *et al*, 2014). Followed by microCT scanning, femurs were

 

dehydrated and embedded in methyl methacrylate. Five-μm-thick sections were prepared using a Leica RM2235 microtome and were stained by the von Kossa/nuclear fast red method. Histomorphometric measurements in the distal end of femurs were made using OsteoMeasure software (OsteoMetrics, Decatur, GA). All histomorphometric parameters were calculated and expressed according to the suggestions made by the ASBMR nomenclature committee (Dempster *et al*, 2013).

#### ELISA

Serum concentrations of P1NP and CTX were measured using ELISA kits from IDS (Fountain Hills, AZ). Animals were fasted for 4 h, and then, blood was collected by puncturing the cheek pouch.

#### BMP2-induced bone formation

*In vivo* analysis of BMP2-induced bone formation by calvarial injection was conducted as described (Mundy *et al*, 1999; Addison *et al*, 2014). Briefly, 7-day-old pups were subcutaneously injected with 2 μg recombinant BMP2 (PeproTech) or saline (vehicle control) twice a day for 5 days onto the sagittal sutures of calvariae. Animals were sacrificed 9 days after the last injection for analysis of bone formation.

For *in vitro* calvarial organ culture, calvariae harvested from 5-day-old pups were cultured in BGJb medium (Life Technologies) containing 0.1% bovine serum albumin (Sigma), 100 units/ml penicillin, and 100 μg/ml streptomycin (Gibco), supplemented with or without 100 ng/ml BMP2. After 7 days, calvariae were fixed in 10% buffered formalin and decalcified with 10% EDTA for 3 days. Tissue samples were then processed, paraffin-embedded, sectioned, and stained with H&E.

#### Surgeries for femoral fracture and cortical defect

Twelve-week-old mice were anesthetized by intraperitoneal injection of a combination of ketamine (100 mg/kg) and xylazine (10 mg/kg). In addition, buprenorphine (0.05 mg/kg) was given for perioperative analgesia to minimize suffering and pain. Unilateral fractures were generated in the right femurs as described by others (Tsuji *et al*, 2006; Yue *et al*, 2016). Briefly, a metal pin (Ø = 0.45 mm) was introduced into the femoral canal through a medial parapatellar incision and arthrotomy of the knee. After closing the wound, a mid-diaphyseal fracture was produced by using a falling weight apparatus over a three-point bending mechanism. At 10 and 21 days post-fracture, samples were collected for radiography, microCT scanning, and histology analysis. For femoral cortical bone defect, a 1.0 mm hole was generated using a round bur (Komet®, Germany) operating at 10,000 rpm under saline irrigation (Liu *et al*, 2016b,c). Samples were harvested 2 weeks after the surgery.

#### Statistical analysis

All values are expressed as mean ± SEM. Statistically significant differences were evaluated by two-tailed Student's *t*-test for comparison between two groups or by one-way analysis of variance (ANOVA) followed by the Tukey's *post hoc* test for multiple comparisons. A *P*-value of less than 0.05 was considered to be statistically significant.

## Data availability

All Seq data have been deposited into NCBI database with the identifier GSE114933, http://www.ncbi.nlm.nih.gov/geo/query/acc.cgi?acc=GSE114933.

**Expanded View** for this article is available online.

### Acknowledgements
We thank Dr. Weiguo Zou from Institute of Biochemistry and Cell Biology, Shanghai, for valuable advices. This work was partly supported by grants from the National Natural Science Foundation of China (NSFC 81722014, 81571001) and Sichuan Province Science and Technology Innovation Team Program (2017TD0016) to Q.Y.; by project of Innovative Research Team of Education Department of Sichuan Province (13TD0038) to L.Y.; and by grants from NSFC (81621062) and 111 Project of Ministry of Education of China to Q.C.

### Author contributions
YG, LY, QC, and QY designed the project; YG, MW, SZ, YW, CZ, RZ, BS, LX, and WL performed experiments; YG, SZ, MW, YW, CZ, NS, JJ, and QY analyzed the data; YG, YW, QC, and QY wrote and edited the manuscript. All authors reviewed the manuscript.

### Conflict of interest
The authors declare that they have no conflict of interest.

## References

Addison WN, Fu MM, Yang HX, Lin Z, Nagano K, Gori F, Baron R (2014) Direct transcriptional repression of Zfp423 by Zfp521 mediates a bone morphogenic protein-dependent osteoblast versus adipocyte lineage commitment switch. *Mol Cell Biol* 34: 3076 – 3085

Bianco P, Robey PG, Simmons PJ (2008) Mesenchymal stem cells: revisiting history, concepts, and assays. *Cell Stem Cell* 2: 313 – 319

Bouxsein ML, Boyd SK, Christiansen BA, Guldberg RE, Jepsen KJ, Muller R (2010) Guidelines for assessment of bone microstructure in rodents using micro-computed tomography. *J Bone Miner Res* 25: 1468 – 1486

Caplan AI (1991) Mesenchymal stem cells. *J Orthop Res* 9: 641 – 650

Caplan AI (2007) Adult mesenchymal stem cells for tissue engineering versus regenerative medicine. *J Cell Physiol* 213: 341 – 347

Cheng X, Alborzinia H, Merz KH, Steinbeisser H, Mrowka R, Scholl C, Kitanovic I, Eisenbrand G, Wolfl S (2012) Indirubin derivatives modulate TGFbeta/BMP signaling at different levels and trigger ubiquitin-mediated depletion of nonactivated R-Smads. *Chem Biol* 19: 1423 – 1436

Ciechanover A (2005) Intracellular protein degradation: from a vague idea, through the lysosome and the ubiquitin-proteasome system, and onto human diseases and drug targeting (Nobel lecture). *Angew Chem Int Ed Engl* 44: 5944 – 5967

Crane JL, Cao X (2014) Bone marrow mesenchymal stem cells and TGF-beta signaling in bone remodeling. *J Clin Invest* 124: 466 – 472

Dempster DW, Compston JE, Drezner MK, Glorieux FH, Kanis JA, Malluche H, Meunier PJ, Ott SM, Recker RR, Parfitt AM (2013) Standardized nomenclature, symbols, and units for bone histomorphometry: a 2012

update of the report of the ASBMR Histomorphometry Nomenclature Committee. *J Bone Miner Res* 28: 2 – 17

Elefteriou F, Yang X (2011) Genetic mouse models for bone studies–strengths and limitations. *Bone* 49: 1242 – 1254

Frith J, Genever P (2008) Transcriptional control of mesenchymal stem cell differentiation. *Transfus Med Hemother* 35: 216 – 227

Grayson WL, Bunnell BA, Martin E, Frazier T, Hung BP, Gimble JM (2015) Stromal cells and stem cells in clinical bone regeneration. *Nat Rev Endocrinol* 11: 140 – 150

James AW (2013) Review of signaling pathways governing MSC osteogenic and adipogenic differentiation. *Scientifica (Cairo)* 2013: 684736

Jones DC, Wein MN, Oukka M, Hofstaetter JG, Glimcher MJ, Glimcher LH (2006) Regulation of adult bone mass by the zinc finger adapter protein Schnurri-3. *Science* 312: 1223 – 1227

Komander D (2009) The emerging complexity of protein ubiquitination. *Biochem Soc Trans* 37: 937 – 953

Komander D, Clague MJ, Urbe S (2009) Breaking the chains: structure and function of the deubiquitinases. *Nat Rev Mol Cell Biol* 10: 550 – 563

Komori T, Yagi H, Nomura S, Yamaguchi A, Sasaki K, Deguchi K, Shimizu Y, Bronson RT, Gao YH, Inada M, Sato M, Okamoto R, Kitamura Y, Yoshiki S, Kishimoto T (1997) Targeted disruption of Cbfa1 results in a complete lack of bone formation owing to maturational arrest of osteoblasts. *Cell* 89: 755 – 764

Korchynskyi O, ten Dijke P (2002) Identification and functional characterization of distinct critically important bone morphogenetic protein-specific response elements in the Id1 promoter. *J Biol Chem* 277: 4883 – 4891

Lee OK, Kuo TK, Chen WM, Lee KD, Hsieh SL, Chen TH (2004) Isolation of multipotent mesenchymal stem cells from umbilical cord blood. *Blood* 103: 1669 – 1675

Li X, Huang M, Zheng H, Wang Y, Ren F, Shang Y, Zhai Y, Irwin DM, Shi Y, Chen D, Chang Z (2008) CHIP promotes Runx2 degradation and negatively regulates osteoblast differentiation. *J Cell Biol* 181: 959 – 972

Liu S, de Boeck M, van Dam H, Ten Dijke P (2016a) Regulation of the TGF-beta pathway by deubiquitinases in cancer. *Int J Biochem Cell Biol* 76: 135 – 145

Liu W, Kang N, Seriwatanachai D, Dong Y, Zhou L, Lin Y, Ye L, Liang X, Yuan Q (2016b) Chronic kidney disease impairs bone defect healing in rats. *Sci Rep* 6: 23041

Liu W, Zhou L, Zhou C, Zhang S, Jing J, Xie L, Sun N, Duan X, Jing W, Liang X, Zhao H, Ye L, Chen Q, Yuan Q (2016c) GDF11 decreases bone mass by stimulating osteoclastogenesis and inhibiting osteoblast differentiation. *Nat Commun* 7: 12794

Logan M, Martin JF, Nagy A, Lobe C, Olson EN, Tabin CJ (2002) Expression of Cre Recombinase in the developing mouse limb bud driven by a Prxl enhancer. *Genesis* 33: 77 – 80

Logeart-Avramoglou D, Bourguignon M, Oudina K, Ten Dijke P, Petite H (2006) An assay for the determination of biologically active bone morphogenetic proteins using cells transfected with an inhibitor of differentiation promoter-luciferase construct. *Anal Biochem* 349: 78 – 86

Lui TT, Lacroix C, Ahmed SM, Goldenberg SJ, Leach CA, Daulat AM, Angers S (2011) The ubiquitin-specific protease USP34 regulates axin stability and Wnt/beta-catenin signaling. *Mol Cell Biol* 31: 2053 – 2065

Malhotra S, Hu MS, Marshall CD, Leavitt T, Cheung AT, Gonzalez JG, Kaur H, Lorenz HP, Longaker MT (2016) Mesenchymal stromal cells as cell-based therapeutics for wound healing. *Stem Cells Int* 2016: 4157934

Mendez-Ferrer S, Michurina TV, Ferraro F, Mazloom AR, Macarthur BD, Lira SA, Scadden DT, Ma'ayan A, Enikolopov GN, Frenette PS (2010) Mesenchymal and haematopoietic stem cells form a unique bone marrow niche. *Nature* 466: 829 – 834

Mundy G, Garrett R, Harris S, Chan J, Chen D, Rossini G, Boyce B, Zhao M, Gutierrez G (1999) Stimulation of bone formation *in vitro* and in rodents by statins. *Science* 286: 1946 – 1949

Otto F, Thornell AP, Crompton T, Denzel A, Gilmour KC, Rosewell IR, Stamp GW, Beddington RS, Mundlos S, Olsen BR, Selby PB, Owen MJ (1997) Cbfa1, a candidate gene for cleidocranial dysplasia syndrome, is essential for osteoblast differentiation and bone development. *Cell* 89: 765 – 771

Ouyang Z, Chen Z, Ishikawa M, Yue X, Kawanami A, Leahy P, Greenfield EM, Murakami S (2014) Prx1 and 3.2 kb Col1a1 promoters target distinct bone cell populations in transgenic mice. *Bone* 58: 136 – 145

Pittenger MF, Mackay AM, Beck SC, Jaiswal RK, Douglas R, Mosca JD, Moorman MA, Simonetti DW, Craig S, Marshak DR (1999) Multilineage potential of adult human mesenchymal stem cells. *Science* 284: 143 – 147

Raggatt LJ, Partridge NC (2010) Cellular and molecular mechanisms of bone remodeling. *J Biol Chem* 285: 25103 – 25108

Rahman MS, Akhtar N, Jamil HM, Banik RS, Asaduzzaman SM (2015) TGF-beta/BMP signaling and other molecular events: regulation of osteoblastogenesis and bone formation. *Bone Res* 3: 15005

Rodda SJ, McMahon AP (2006) Distinct roles for Hedgehog and canonical Wnt signaling in specification, differentiation and maintenance of osteoblast progenitors. *Development* 133: 3231 – 3244

Rodriguez-Carballo E, Ulsamer A, Susperregui AR, Manzanares-Cespedes C, Sanchez-Garcia E, Bartrons R, Rosa JL, Ventura F (2011) Conserved regulatory motifs in osteogenic gene promoters integrate cooperative effects of canonical Wnt and BMP pathways. *J Bone Miner Res* 26: 718 – 729

Sacchetti B, Funari A, Michienzi S, Di Cesare S, Piersanti S, Saggio I, Tagliafico E, Ferrari S, Robey PG, Riminucci M, Bianco P (2007) Self-renewing osteoprogenitors in bone marrow sinusoids can organize a hematopoietic microenvironment. *Cell* 131: 324 – 336

Salazar VS, Gamer LW, Rosen V (2016) BMP signalling in skeletal development, disease and repair. *Nat Rev Endocrinol* 12: 203 – 221

Schaffler A, Buchler C (2007) Concise review: adipose tissue-derived stromal cells–basic and clinical implications for novel cell-based therapies. *Stem Cells* 25: 818 – 827

Severe N, Dieudonne FX, Marie PJ (2013) E3 ubiquitin ligase-mediated regulation of bone formation and tumorigenesis. *Cell Death Dis* 4: e463

Sharpe PT (2016) Dental mesenchymal stem cells. *Development* 143: 2273 – 2280

Shu L, Zhang H, Boyce BF, Xing L (2013) Ubiquitin E3 ligase Wwp1 negatively regulates osteoblast function by inhibiting osteoblast differentiation and migration. *J Bone Miner Res* 28: 1925 – 1935

Sims NA, Martin TJ (2014) Coupling the activities of bone formation and resorption: a multitude of signals within the basic multicellular unit. *Bonekey Rep* 3: 481

Song L, Liu M, Ono N, Bringhurst FR, Kronenberg HM, Guo J (2012) Loss of wnt/beta-catenin signaling causes cell fate shift of preosteoblasts from osteoblasts to adipocytes. *J Bone Miner Res* 27: 2344 – 2358

Trapnell C, Roberts A, Goff L, Pertea G, Kim D, Kelley DR, Pimentel H, Salzberg SL, Rinn JL, Pachter L (2012) Differential gene and transcript expression analysis of RNA-seq experiments with TopHat and Cufflinks. *Nat Protoc* 7: 562 – 578

Tsuji K, Bandyopadhyay A, Harfe BD, Cox K, Kakar S, Gerstenfeld L, Einhorn T, Tabin CJ, Rosen V (2006) BMP2 activity, although dispensable for bone formation, is required for the initiation of fracture healing. *Nat Genet* 38: 1424 – 1429

 

Vriend J, Reiter RJ (2016) Melatonin, bone regulation and the ubiquitin-proteasome connection: a review. *Life Sci* 145: 152 – 160

Williams SA, Maecker HL, French DM, Liu J, Gregg A, Silverstein LB, Cao TC, Carano RA, Dixit VM (2011) USP1 deubiquitinates ID proteins to preserve a mesenchymal stem cell program in osteosarcoma. *Cell* 146: 918 – 930

Wu M, Chen G, Li YP (2016) TGF-beta and BMP signaling in osteoblast, skeletal development, and bone formation, homeostasis and disease. *Bone Res* 4: 16009

Xiong J, Onal M, Jilka RL, Weinstein RS, Manolagas SC, O'Brien CA (2011) Matrix-embedded cells control osteoclast formation. *Nat Med* 17: 1235 – 1241

Yamashita M, Ying SX, Zhang GM, Li C, Cheng SY, Deng CX, Zhang YE (2005) Ubiquitin ligase Smurf1 controls osteoblast activity and bone homeostasis by targeting MEKK2 for degradation. *Cell* 121: 101 – 113

Ye Y, Pringle LM, Lau AW, Riquelme DN, Wang H, Jiang T, Lev D, Welman A, Blobel GA, Oliveira AM, Chou MM (2010) TRE17/USP6 oncogene translocated in aneurysmal bone cyst induces matrix metalloproteinase production via activation of NF-kappaB. *Oncogene* 29: 3619 – 3629

Yuan Q, Sato T, Densmore M, Saito H, Schuler C, Erben RG, Lanske B (2012) Deletion of PTH rescues skeletal abnormalities and high osteopontin levels in Klotho-/- mice. *PLoS Genet* 8: e1002726

Yuan Q, Jiang Y, Zhao X, Sato T, Densmore M, Schuler C, Erben RG, McKee MD, Lanske B (2014) Increased osteopontin contributes to inhibition of bone mineralization in FGF23-deficient mice. *J Bone Miner Res* 29: 693 – 704

Yue R, Zhou BO, Shimada IS, Zhao Z, Morrison SJ (2016) Leptin receptor promotes adipogenesis and reduces osteogenesis by regulating mesenchymal stromal cells in adult bone marrow. *Cell Stem Cell* 18: 782 – 796

Zaidi M (2007) Skeletal remodeling in health and disease. *Nat Med* 13: 791 – 801

Zhao M, Qiao M, Oyajobi BO, Mundy GR, Chen D (2003) E3 ubiquitin ligase Smurf1 mediates core-binding factor alpha1/Runx2 degradation and plays a specific role in osteoblast differentiation. *J Biol Chem* 278: 27939 – 27944

Zhao M, Qiao M, Harris SE, Oyajobi BO, Mundy GR, Chen D (2004) Smurf1 inhibits osteoblast differentiation and bone formation *in vitro* and *in vivo*. *J Biol Chem* 279: 12854 – 12859

Zhao L, Huang J, Guo R, Wang Y, Chen D, Xing L (2010) Smurf1 inhibits mesenchymal stem cell proliferation and differentiation into osteoblasts through JunB degradation. *J Bone Miner Res* 25: 1246 – 1256

Zhou F, Li F, Fang P, Dai T, Yang B, van Dam H, Jia J, Zheng M, Zhang L (2016) Ubiquitin-specific protease 4 antagonize osteoblast differentiation through dishevelled. *J Bone Miner Res* 31: 1888 – 1898

Zhou CC, Xiong QC, Zhu XX, Du W, Deng P, Li XB, Jiang YZ, Zou SJ, Wang CY, Yuan Q (2017) AFF1 and AFF4 differentially regulate the osteogenic differentiation of human MSCs. *Bone Res* 5: 17044

Zhu H, Kavsak P, Abdollah S, Wrana JL, Thomsen GH (1999) A SMAD ubiquitin ligase targets the BMP pathway and affects embryonic pattern formation. *Nature* 400: 687 – 693